Volume 11
Number 7
7 April 2023
Pages 2255-2608

Biomaterials Science

rsc.li/biomaterials-science

ISSN 2047-4849

ROYAL SOCIETY OF CHEMISTRY

PAPER
Sabina Quader,
Rosalía Rodríguez-Rodríguez *et al.*
Nanomedicine targeting brain lipid metabolism as a feasible approach for controlling the energy balance

10 YEARS ANNIVERSARY

ESB European Society for Biomaterials

Biomaterials Science

ROYAL SOCIETY OF CHEMISTRY

PAPER

View Article Online
View Journal | View Issue

Cite this: *Biomater. Sci.*, 2023, **11**, 2336

Nanomedicine targeting brain lipid metabolism as a feasible approach for controlling the energy balance†

Jesús Garcia-Chica,‡[a] West Kristian Dizon Paraiso, ‡§[b] Sebastián Zagmutt,[a] Anna Fosch,[a] Ana Cristina Reguera,[a] Sara Alzina,[a] Laura Sánchez-García,[a] Shigeto Fukushima,[b] Kazuko Toh,[b] Núria Casals,[a,c] Dolors Serra, [c,d] Laura Herrero,[c,d] Jordi Garcia, [c,e] Kazunori Kataoka,[b] Xavier Ariza, [c,e] Sabina Quader *[b] and Rosalía Rodríguez-Rodríguez *[a,c]

Received 27th October 2022,
Accepted 3rd January 2023

DOI: 10.1039/d2bm01751b

rsc.li/biomaterials-science

Targeting brain lipid metabolism is a promising strategy to regulate the energy balance and fight metabolic diseases such as obesity. The development of stable platforms for selective delivery of drugs, particularly to the hypothalamus, is a challenge but a possible solution for these metabolic diseases. Attenuating fatty acid oxidation in the hypothalamus *via* CPT1A inhibition leads to satiety, but this target is difficult to reach *in vivo* with the current drugs. We propose using an advanced crosslinked polymeric micelle-type nanomedicine that can stably load the CPT1A inhibitor C75-CoA for *in vivo* control of the energy balance. Central administration of the nanomedicine induced a rapid attenuation of food intake and body weight in mice *via* regulation of appetite-related neuropeptides and neuronal activation of specific hypothalamic regions driving changes in the liver and adipose tissue. This nanomedicine targeting brain lipid metabolism was successful in the modulation of food intake and peripheral metabolism in mice.

New concepts

Effective treatments to control feeding, body weight, and glucose homeostasis in metabolic diseases such as obesity or diabetes are insufficient, due to the difficulty of reaching specific brain targets that are in charge of energy balance. Here, we present the first nanomedicine acting on a brain target to drive a rapid modulation of food intake and peripheral metabolism, offering an innovative approach to managing metabolic diseases. The core-crosslinked polymeric micelle-based nanomedicine used in this investigation allows the encapsulation of a drug that modifies lipid metabolism in the brain, a target hard to reach with conventional formulations. This investigation might contribute to developing and validating a new generation of nanomedicine-based approaches targeting brain lipid metabolism to modulate feeding and body weight. Also, this nanomedicine highlights the significance of nanotechnology beyond the current biological applications and facilitates the understanding of the early stages of energy balance (*i.e.*, acute satiating actions) that are crucial for developing complex diseases such as obesity and diabetes.

1. Introduction

Metabolic disorders such as obesity imply a disruption in energy homeostasis, leading to an imbalance between food intake and energy expenditure.[1] Despite the major advances in understanding the pathogenesis and therapeutics of these metabolic disorders, the prevalence of obesity and type 2 diabetes continues to rise.[2,3] Against this backdrop, these metabolic diseases have still unmet medical needs and require the development of new therapeutic platforms.

[a]*Basic Sciences Department, Faculty of Medicine and Health Sciences, Universitat Internacional de Catalunya (UIC), Sant Cugat del Vallès, E-08195, Spain. E-mail: rrodriguez@uic.es; Tel: +34-935-042-002*
[b]*Innovation Center of Nanomedicine, Kawasaki Institute of Industrial Promotion, Kawasaki, Kanagawa 210-0821, Japan. E-mail: sabina-q@kawasaki-net.ne.jp; Tel: +81-44-589-5920*
[c]*Centro de Investigación Biomédica en Red de Fisiopatología de la Obesidad y la Nutrición (CIBEROBN), Instituto de Salud Carlos III, Madrid, E-28029, Spain*
[d]*Department of Biochemistry and Physiology, School of Pharmacy and Food Sciences, Institut de Biomedicina de la Universitat de Barcelona (IBUB), Universitat de Barcelona, Barcelona, E-08028, Spain*
[e]*Department of Inorganic and Organic Chemistry, Faculty of Chemistry, Institut de Biomedicina de la Universitat de Barcelona (IBUB), Universitat de Barcelona (UB), Barcelona, E-08028, Spain*

†Electronic supplementary information (ESI) available. See DOI: **https://doi.org/10.1039/d2bm01751b**

‡These authors contributed equally to this work.

§Present address: Red Arrow Therapeutics Co., Ltd, Tokyo 113-0033, Japan.

The physiological control of energy balance is tightly modulated by the central nervous system (CNS), where the hypothalamus is the most critical area implicated.[4,5] Hypothalamic nuclei are sensitive to nutrients and hormones and modify the expression, secretion, and activity of specific neurotransmitters and neuromodulators, resulting in changes in food intake, energy expenditure, and the function of key peripheral tissues such as the liver and adipose tissue.[4,6,7] Strong evidence suggests that lipid metabolism within the hypothalamus is a key signal of nutrient status further to modulate feeding behaviour and peripheral metabolism.[8–10] In particular, fatty acid (FA) sensing in hypothalamic neurons *via* accumulation of FAs or FA metabolites acts as a satiety signal and may decrease food intake and hepatic function.[1,11]

A crucial target in brain lipid metabolism which controls the energy balance is carnitine palmitoyl-transferase 1A (CPT1A).[12] It is located in the mitochondria and promotes the entry of long-chain FAs for β-oxidation.[13–16] Since CPT1A is highly expressed in central and peripheral tissues, its regulatory potential in the energy balance is based on two different interventions: in peripheral tissues (*i.e.*, liver and adipose tissue), overexpression of CPT1A and induction of fatty acid oxidation (FAO) ameliorate insulin resistance and prevent body weight gain,[17,18] whereas in the CNS, CPT1A inhibition reduces food intake and body weight.[19,20] Particularly, in the arcuate (ARC) nucleus of the hypothalamus, genetic ablation of CPT1A prevents FAO, leading to a local accumulation of long-chain FAs which in turn mediates the action of several feeding-related hormones to inhibit food intake in lean rats.[21] Thus, selective inhibition of CPT1A in the hypothalamus, but not in the peripheral tissues, is a promising strategy for the management of metabolic disorders involving a disruption in energy balance. However, brain lipid metabolism is difficult to reach *in vivo* with the current formulations and drugs.

(±)-C75 is a well-known CPT1A inhibitor that is converted to its active coenzyme A (CoA) form in the hypothalamus.[22] Although initially identified as a fatty acid synthase (FAS) inhibitor with a strong anorectic effect *via* malonyl-CoA accumulation,[23–25] enantioselective synthesis of C75 revealed that the (+)-C75 and (±)-C75-CoA adducts were the active forms inhibiting CPT1A.[22,26] Therefore, to avoid the off-target effect on FAS and undesired actions in the periphery, it is crucial to deliver (±)-C75-CoA directly into the brain for CPT1A inhibition and energy balance regulation. A major challenge of (±)-C75-CoA as cargo is that it is a small, polar, and negatively charged molecule, with low permeability across the cellular membrane. (±)-C75-CoA interacts with polycations through a combination of electrostatic and hydrophobic interactions, as it possesses both phosphate and carboxylate groups, as well as an aliphatic side chain.[27] We used this particular property in designing a poly-ion complex (PIC) micelle, a polymeric formulation that allows for a direct and specific cellular transport of (±)-C75-CoA, demonstrating an efficient inhibition of CPT1A-dependent lipid metabolism in cellular models of neurons and glioma cells.[28] In the present study, we have developed a more robust core-crosslinked polymeric micelle (PM)-type nanomedicine, with a high entrapment efficiency of the specific CPT1A inhibitor (±)-C75-CoA (Fig. 1). This crosslinked PM has proven to be useful for *in vivo* applications, showing an effective biological activity upon delivery of the CPT1A inhibitor in brain cells after intracerebroventricular (ICV) administration, particularly to neurons. In addition, central administration of this (±)-C75-CoA-loaded core-crosslinked PM induced a substantial reduction in food intake and body weight in mice as compared to the free drug, as well as significant regulation of appetite-related neuropeptides, neuronal activation of specific hypothalamic regions and altered expression of metabolic biomarkers in peripheral tissues (Fig. 1). This investigation led to the first nanomedicine targeting brain lipid metabolism, which effectively modulated energy intake and peripheral tissue metabolism.

2. Results and discussion

2.1 Stability of crosslinked polymeric micelles (PM) loading (±)-C75-CoA and uptake in neuronal cell lines

In this study, we synthesized a triblock co-polymer using sequential *N*-carboxyanhydride (NCA) polymerization with polyethylene glycol (PEG) as a hydrophilic shell forming block, a poly(L-aspartamide) (PAsp) middle block functionalized *via* an orthogonal side-chain modification with an aromatic aldehyde moiety (PAsp(Aldehyde)), and a poly(L-lysine) (PLys) cationic block designed to form a PIC with (±)-C75-CoA (Fig. 2). Solutions of (±)-C75-CoA and PEG-PAsp(Aldehyde)-PLys were combined in a 1 : 1 anion/cation ratio, defined as the ratio between the overall anionic charge imparted by the phosphate and carboxylate groups in (±)-C75-CoA and the overall cationic charge given by the protonated amines in the polymer. A PEG-PAsp diblock co-polymer functionalized with hydrazide groups (PEG-PAsp(Hydrazide)) was added to the micelle to crosslink the aldehyde-containing PEG-PAsp(Aldehyde)-PLys through hydrazone formation (Fig. 1). This aromatic aldehyde and hydrazide-derived reversible hydrazone bonds[29,30] formed in the copolymer middle block provided increased protection and stability to the micelle by tightening the core and preventing premature release of the cargo (Fig. 1). (±)-C75-CoA and PEG-PAsp(Aldehyde)-PLys were mixed in 10 mM phosphate buffer (pH 7.4) that spontaneously self-assembled to form a core–shell structured PM. To crosslink the PM, PEG-PAsp (Hydrazide) was added in molar equivalence of hydrazide to the aldehyde functionality (Fig. 1). Upon filtration, both non-crosslinked and crosslinked PMs gave monodisperse size profiles of around 40–45 nm hydrodynamic diameter, determined by dynamic light scattering (DLS) measurements (Fig. 3A; ESI Table S1†). In comparison, the average core size of PMs was found to be *ca.* 20 nm by transmission electron microscopy (TEM), which is smaller than the hydrodynamic diameter, since the latter accounts for the PEG shell of the micelle (Fig. S1, ESI†). It is worth highlighting that the middle block strengthens the micelle core even without crosslinking, possibly by providing hydrophobicity.[31] The polymer mixtures only

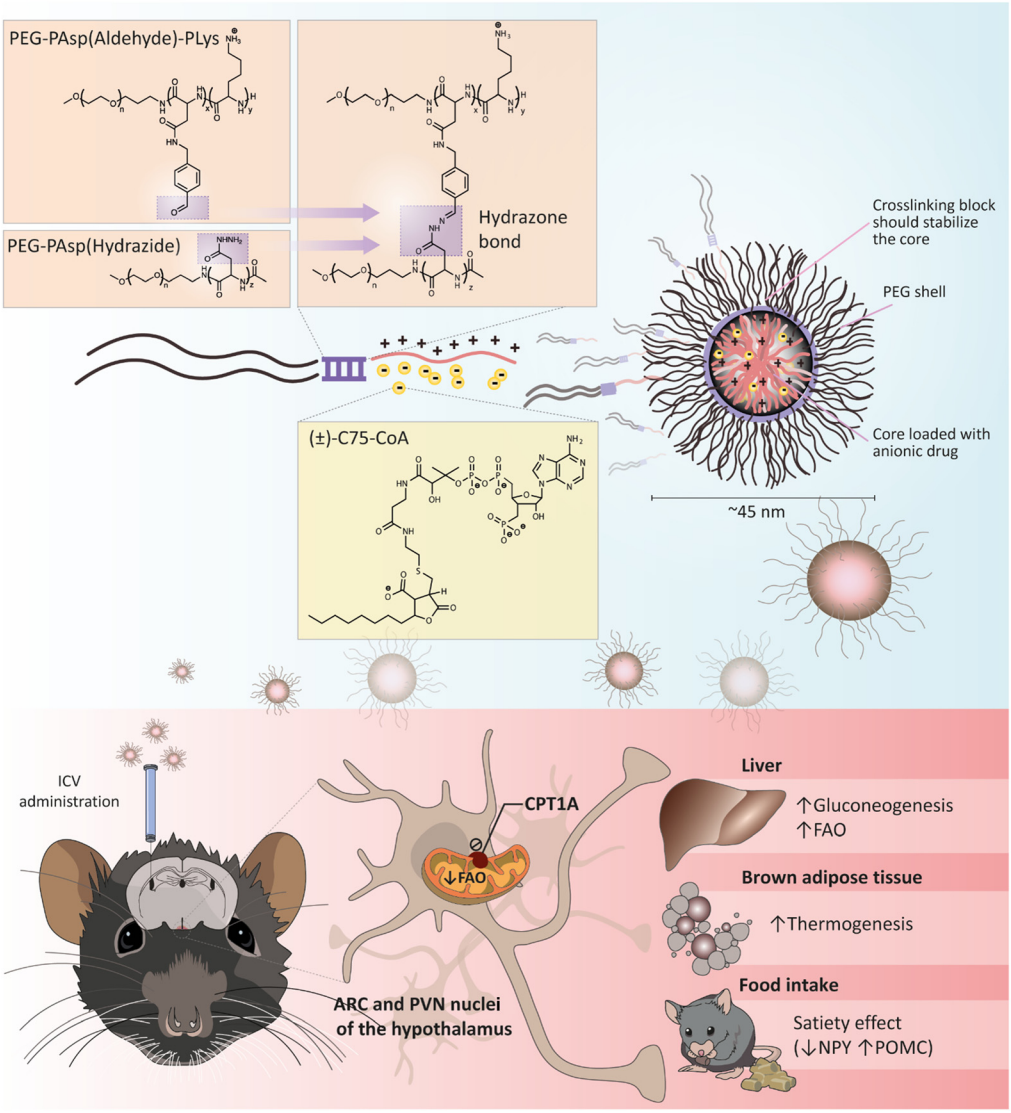

Fig. 1 Schematic representation of the core-crosslinked polymeric micelle (PM)-type nanomedicine encapsulating the CPT1A inhibitor (±)-C75-CoA, and the effects of central administration (ICV) of the nanomedicine on food intake and liver and brown fat metabolism *via* the arcuate (ARC) and paraventricular (PVN) nuclei of the hypothalamus.

(without (±)-C75-CoA) provided large aggregates, confirming that the cargo has a profound influence in producing well-defined PM-type structures, which was evident from the TEM images (Fig. S1, ESI†).

To confirm the advantages of the middle block, we prepared micelles from a PEG-PLys diblock copolymer (Fig. S2A, ESI†). We then added a polyanion (sodium dextran sulfate; DSS) to confirm the ionic interaction between the anionic cargo and the cationic PLys chain. Micelle dissociation with the increase of DSS concentration was observed for the diblock PM, evident by the drastic reduction of light scattering intensity, but for that of the triblock PM the impact of DSS addition was minimal (Fig. S2B, ESI†). A core-crosslinked PM prepared from the PEG-PAsp(Aldehyde)-PLys triblock and PEG-PAsp (Hydrazide) diblock co-polymer incorporating crosslinking to provide hydrophobicity is expected to give even higher stability. To confirm the participation of these two polymers in the micellar assembly and subsequent interaction, we labelled the PEG-PAsp(Aldehyde)-PLys polymer with rhodamine and PEG-PAsp(Hydrazide) with fluorescein on their N-termini. When the labelled polymers were used to form PMs with (±)-C75-CoA, we observed Förster resonance energy transfer (FRET) upon scanning the emitted light at 450 nm excitation (Fig. 3B), corroborating that they were associated with the PM core. The FRET profile of crosslinked PMs was not altered with the addition of 1 M NaCl. However, upon adding DSS, the signal intensity from the rhodamine-labelled polymer was reduced to 60%, which indicated that (±)-C75-CoA plays a significant role in the association of two polymers, as evidenced by FRET pairing. To further confirm whether (±)-C75-CoA was necessary for the increased interaction of the FRET-paired polymers, the FRET spectrum of a mixture of the two labelled

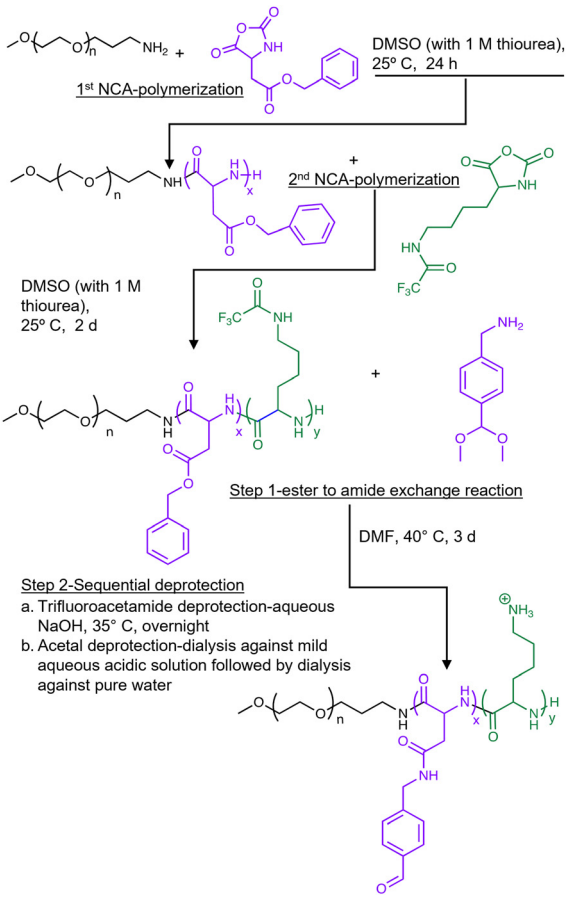

Fig. 2 Preparation of the triblock polymer, PEG-PAsp(Aldehyde)-PLys.

polymers was measured. This revealed similar FRET properties to those of the DSS-treated PM. However, when the FRET-paired polymers were mixed without (±)-C75-CoA and then treated with DSS, a residual FRET signal was observed. This suggests that there was still some form of interaction between the two polymers despite the release/absence of the (±)-C75-CoA cargo, possibly through covalent (hydrazone) bonds and other forces of attraction.

To check micellar stability in salt solution, we added 1 M NaCl to the PM solution. This led to a 15 nm increase in size for both types of micelles (Fig. 3C); however, the non-crosslinked PM gave an apparently more polydisperse size profile with a statistical decrease in scattered light intensity (Fig. 3D and E). The results attested to the PIC nature of the PM. PIC formation is mainly driven by the liberation of counterions,[32] which is prompted when the PLys block and anionic (±)-C75-CoA paired up, leading to a large entropic gain. The increased NaCl concentration apparently reduced this entropic gain, which resulted in PIC destabilization. These data provide additional evidence that the crosslinked PM is more stable than the non-crosslinked PM.

To test their differing effects on biological systems, we measured the ATP synthesis of GT1-7 mouse hypothalamic neurons after short-term incubation with the PMs. This is an indirect approach to measure mitochondria FAO and CPT1A inhibition by the drug[28] (Fig. 3F). The crosslinked PM statistically reduced cellular ATP production to 41%, as compared to the non-crosslinked PM (73%) and free (±)-C75-CoA (87%) (Fig. 3F). Moderation of the ATP synthesis in *in vitro* neurons in response to PM treatment indicates inhibition of FAO, in agreement with the previous data,[28,33] and this attenuation was significantly higher compared to the non-crosslinked PM. The crosslinked PM exhibited higher apparent encapsulation of (±)-C75-CoA compared to the non-crosslinked PM in both pH 7.4 phosphate buffer (PB) and artificial cerebrospinal fluid (aCSF) (Fig. S3, ESI†), with the latter mimicking conditions in the brain. Since more (±)-C75-CoA was entrapped in the crosslinked PM, it was expected to enter the cell more efficiently in contrast to the non-crosslinked PM.

To track its cellular uptake, we prepared PMs from a fluorescent derivative of CoA, Fluor-CoA,[28] with a size profile similar to (±)-C75-CoA-PM (Fig. S4A, ESI†). Upon incubation with GT1-7 neuronal cells for 30 min, we observed that there was an evidently higher cellular uptake of Fluor-CoA-loaded crosslinked PM (4× that of the free dye) as compared with the non-crosslinked PM (3× compared to the free dye) (Fig. 3G). This points to another reason why the crosslinked PM has a greater ATP inhibitory effect compared to the non-crosslinked counterpart. Fluor-CoA was also released in the cell culture medium or aCSF to a lesser extent by the crosslinked PM (Fig. S4C and D, ESI†), despite both non-crosslinked and crosslinked PM having similar encapsulation rates (Fig. S4B, ESI†). In neuronal cells, the fluorescent tracer of the micelle showed *endo*-lysosomal entrapment, which was not appreciated in the mitochondria (Fig. S5, ESI†).

The increased stability of the crosslinked PM ensured a higher (±)-C75-CoA encapsulation rate, an enhanced ATP inhibitory capacity, and increased cellular uptake of fluorescein when using the Fluor-CoA-loaded PM. This cellular uptake was also confirmed *in vivo*, since the brain slices revealed fluorescent staining of the tracer of the crosslinked PM, particularly in the hypothalamic area, after ICV infusion of the nanomedicine (Fig. S6, ESI†), as previously indicated with other types of polymeric nanomedicines.[48–50]

Altogether, the formulation presented here, which is based on a specially designed triblock copolymer platform, allowed for remarkable stability better suited for *in vivo* applications when matched with the non-crosslinked PM. This could be explained by: (i) increased hydrophobicity of the polymer, which enabled a better interaction with (±)-C75-CoA and (ii) crosslinking of the two polymers through hydrazone formation. The polymer PEG chain (M_W 12 kDa) was important in imparting the measured physicochemical properties and decreasing aggregation tendency.[32]

2.2 (±)-C75-CoA-loaded core crosslinked PMs induced rapid attenuation of food intake and body weight and regulated the expression of hypothalamic neuropeptides

A major finding of this investigation is the remarkable acute effect of the central administration of the nanomedicine on feeding and body weight, with improvements in these actions

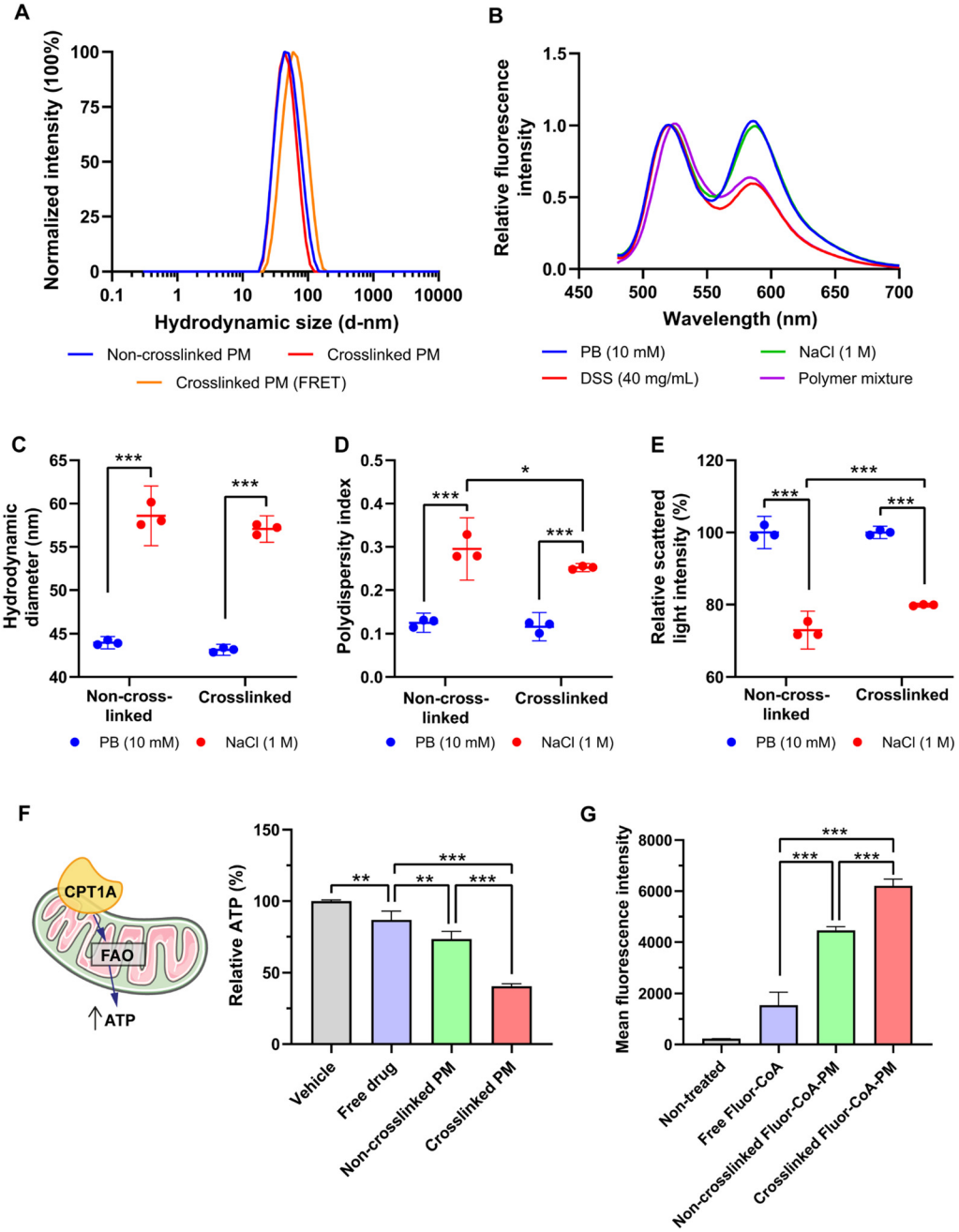

Fig. 3 Physicochemical characterization of the crosslinked polymeric micelles (PMs) loading (±)-C75-CoA or Fluor-CoA and validation in the neuronal cell lines. (A) Size profile of (±)-C75-CoA-PM. (B) Fluorescence emission spectra of the FRET double-labelled (±)-C75-CoA-PM and mixed polymers. (C–E) Physicochemical properties of the micelles in phosphate buffer (PB) and NaCl solution: (C) hydrodynamic size, (D) polydispersity, and (E) scattered light intensity of non-crosslinked *versus* crosslinked PM. (F) Measurement of ATP levels as an indirect indicator of fatty acid oxidation (FAO) and CPT1A activity in neuronal cells treated with the vehicle, free drug, non-crosslinked and crosslinked-PM. (G) Cellular uptake of Fluor-CoA non-crosslinked or crosslinked micelles. Data are expressed as mean ± SD (n = 3–4). Means were compared using one-way ANOVA along with Tukey's *post hoc* test. *p < 0.05, **p < 0.01 and ***p < 0.001.

compared to the free drug (±)-C75 administration. In these experiments, age-matched mice were administered ICV injections of the vehicle: (±)-C75, (±)-C75-CoA, and (±)-C75-CoA-loaded core crosslinked PMs (from here on will be designated as (±)-C75-CoA-PM). Food intake and body weight were then monitored for 24 h (Fig. 4A). This timing was in agreement with the previous studies monitoring the acute satiating effects of new therapeutics in lean rodent models.[13,34,35] Mice treated with (±)-C75-CoA-PM exhibited a substantial and rapid reduction of food intake in comparison with (±)-C75-CoA-, (±)-C75- and vehicle-treated mice (Fig. 4B). The satiating effect of (±)-C75-CoA-PM was appreciated after 1 h, being statistically

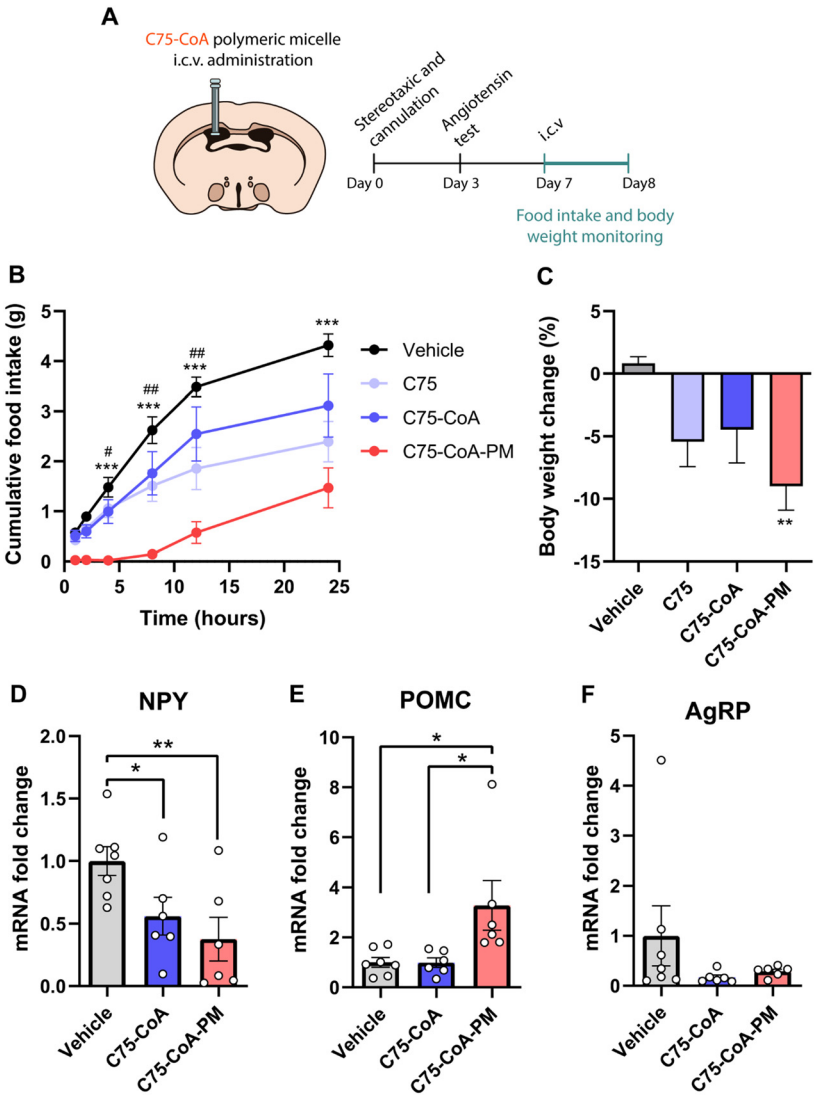

Fig. 4 ICV administration of (±)-C75-CoA polymeric micelles (PM) rapidly reduced food intake and body weight in mice by regulating the expression of hypothalamic neuropeptides. (A) Diagram indicating the experimental protocol of surgery, administration and monitoring. (B) Cumulative food intake at different timings (***$p < 0.001$ *vs.* (±)-C75-CoA-PM; $^{\#}p < 0.05$ and $^{\#\#}p < 0.01$ *vs.* (±)-C75-CoA) and (C) body weight change in mice after 24 h of central administration of the vehicle, free drug or the nanomedicine ((±)-C75-CoA-PM) (**$p < 0.01$ *vs.* vehicle)). (D–F) mRNA levels of the hypothalamic neuropeptides (D) NPY (orexigenic and energy expenditure inhibitor), (E) POMC (anorexigenic and energy expenditure activator) and (F) AgRP (orexigenic and energy expenditure inhibitor), 2.5 h post-injection (*$p < 0.05$ and **$p < 0.01$). Data are expressed as mean ± SD (n = 6–8). Means were compared using one-way ANOVA along with Tukey's *post hoc* test.

different 4 h post-treatment *versus* the vehicle and free drugs. This action was maintained throughout the experiment (24 h) (Fig. 4B). In line with this result, body weight change measured at 24 h post-treatment was also significantly reduced in (±)-C75-CoA-PM-treated mice when evaluated against the control group (Fig. 4C). These acute effects on energy balance in lean mice are very promising and comparable to the satiating action of CPT1A inhibition after short timings (2 to 24 h) in lean rodents using drug- or genetic-based approaches.[21,23,36] In agreement with the observed rapid effects on feeding, it has been reported that the levels of malonyl-CoA, when elevated in the brain and particularly in the hypothalamus in response to energy surplus or glucose overload, induces rapid inhibition of CPT1A, leading to food intake reduction, and these changes appear very rapidly (from minutes to a few hours).[16,37]

Since alteration of brain CPT1A and malonyl-CoA levels is known to modify the expression of hunger-related neuropeptides in the hypothalamus,[36] we measured the mRNA expression of these neuropeptides. Once released by different neuronal populations in the ARC nucleus of the hypothalamus, the following peptides exert opposing effects on feeding and metabolism: the neuropeptide Y (NPY) and agouti-gene related protein (AgRP) are orexigenic neuropeptides, whereas the precursor protein, proopiomelanocortin (POMC), is a signal that induces satiety and body weight attenuation.[38,39] For this analysis, hypothalamic extracts of mice were collected

2.5 h after the treatment with the vehicle, free drug or PM. These timings were based on previous studies with altering malonyl-CoA levels and CPT1A activity in the hypothalamus, showing very rapid changes in the expression of these neuropeptides (2–3 hours post central inhibition of the target and lipid metabolism).[13,40] While free (±)-C75-CoA was able to attenuate the mRNA levels of the orexigenic neuropeptide NPY, (±)-C75-CoA-PM induced not only a significant reduction of NPY (Fig. 4D), but also upregulation of the anorexigenic neuropeptide POMC compared to the vehicle (Fig. 4E). However, no changes were appreciated in the mRNA levels of AgRP in response to either free drug or PM (Fig. 4F).

Despite our results being too preliminary to discard important side effects in patients with metabolic diseases, the present results are promising in terms of toxicity. In particular, analysis of microglial activation by Iba1 immunofluorescence in different regions of the hypothalamus revealed no activation of microglia after ICV infusion of the nanomedicine, indicating the low toxic potential of the formulation in the inflammatory response at the timing and dose tested in mice (Fig. S7, ESI†). Subsequent investigations using more selective targeting-based approaches to a specific type of neurons and after longer periods of administration to analyse feeding behaviour must be envisaged.

These data suggest that the nanomedicine (±)-C75-CoA-PM was more efficient in reducing body weight and food intake compared to the free drug, and that the appetite-suppressing effect could be explained through the modulation of hunger-related neuropeptides in the hypothalamus, particularly the upregulation of POMC and the downregulation of NPY. The main satiety signal in the brain which led to changes in the expression of neuropeptides meant that there was a local accumulation of long-chain fatty acyl-CoAs in the hypothalamus in response to FAO and CPT1A inhibition, indicating nutrient overload, as previously reported.[9,21]

2.3 (±)-C75-CoA-PM modified liver and brown fat metabolism

The hunger-related hypothalamic neuropeptides released in the ARC nucleus connect to second order neurons located in other hypothalamic nuclei to control energy balance, not only in terms of satiety, but also in terms of liver and adipose tissue metabolism.[41–43] Therefore, the effect of central administration of the drug in the free form or PM form was also investigated in these primary metabolically active tissues. Particularly, markers of glycolysis, gluconeogenesis, and FAO were assayed in the liver (Fig. 5A), while markers of thermogenesis were measured in the brown adipose tissue (BAT) (Fig. 5B) 2.5 h post-ICV injection of either vehicle, free drug, or PM.

In the liver, gluconeogenesis (PEPCK) and FAO (CPT1A) mRNA markers were significantly increased by (±)-C75-CoA-PM in comparison with the free drug or vehicle with no accompanying changes in the last stage of glucose production (G6Pase), which is consistent with a response to a satiating effect (Fig. 5A). In line with this, the expression of the pyruvate kinase liver isoform (PKL), a regulator of pyruvate production, remained unchanged when using (±)-C75-CoA, but was significantly reduced by (±)-C75-CoA-PM, supporting the idea that the nanomedicine can promote FAO and the initial stages of gluconeogenesis, but not pyruvate, to provide energy fuel to extrahepatic tissues in response to the satiating actions.

The analysis of genes related to thermogenesis in the BAT, which contributes to energy expenditure and body weight regulation,[44] revealed significant induction of the expression of several genes involved in BAT thermogenesis activation, probably contributing to energy expenditure and body weight loss after this treatment. In contrast, the free drug was not able to modify the expression of the genes under study (Fig. 5B).

Taken together, these results show that central administration of (±)-C75-CoA-PM led to transcriptional changes in metabolically active tissues in the periphery, such as the liver and BAT, whereas the expression of these markers remained unaffected in free (±)-C75-CoA-treated mice.

2.4 (±)-C75-CA-PM activated neurons in specific hypothalamic nuclei

In order to assess the activation of neurons in different areas of the hypothalamus in response to the free drug or nanomedicine (±)-C75-CoA, c-FOS immunostaining (a proto-onco-

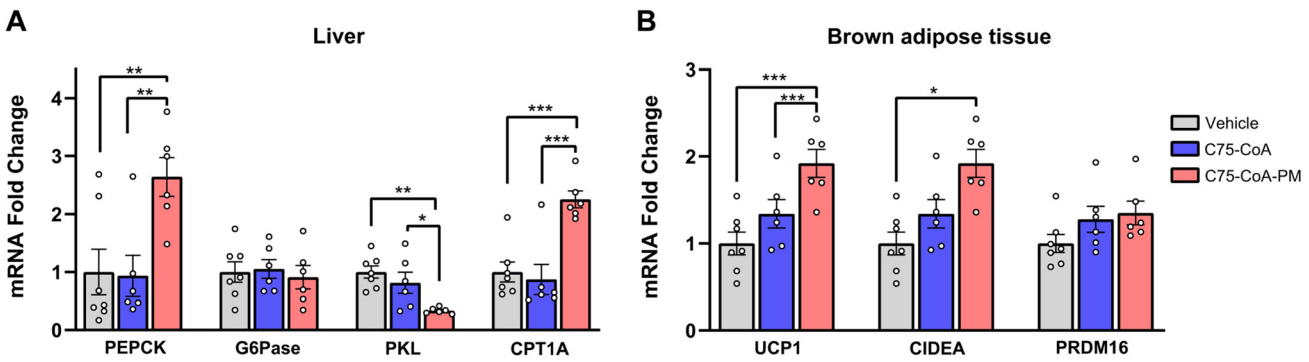

Fig. 5 ICV administration of (±)-C75-CoA polymeric micelles (PM) modifies metabolic pathways in the liver and brown adipose tissue (BAT). (A) Liver mRNA levels of genes involved in gluconeogenesis, glycolysis and fatty acid oxidation. (B) BAT mRNA levels of genes involved in thermogenesis activation. Tissues were collected 2.5 h post-injection of vehicle, free (±)-C75-CoA or (±)-C75-CoA-PM. Data are expressed as mean ± SD (n = 6–8). Means were compared using one-way ANOVA along with Tukey's *post hoc* test; *p < 0.05, **p < 0.01 and ***p < 0.001.

gene expressed within neurons following depolarization, indicating neuronal activity) was explored in the hypothalamus. This analysis was performed in ARC nucleus and paraventricular nucleus (PVN), two major hypothalamic nuclei involved in feeding behavior, liver metabolism and thermogenesis.[41,42] The number of c-FOS positive cells statistically increased in the PVN of (±)-C75-CoA-PM-injected mice as compared to those treated with the vehicle, whereas no changes were seen in mice treated with (±)-C75-CoA (Fig. 6A and B). However, analysis in the ARC revealed a lower level of neuronal activation in mice treated with (±)-C75-CoA *versus* vehicle, whereas (±)-C75-CoA-PM-treated mice showed partial restoration of this activation in parallel to the free drug (Fig. 6C and D).

The differential neuronal activation patterns in the hypothalamic nuclei PVN and ARC in response to the treatments can be explained by the remarkable satiating action and metabolic changes induced by (±)-C75-CoA-PM. Particularly, c-FOS measurements indicated that the nanomedicine could be initiating the following events: (i) stimulation of anorexigenic POMC neurons in the ARC, which led to (ii) activation of the PVN, which drove satiating effects, and (iii) triggering of changes in liver metabolism and BAT thermogenesis to regulate body weight (Fig. 6E). These observations are consistent with the changes in the expression of the neuropeptides POMC and NPY observed with the nanomedicine but not with the free drug. These in turn connect with the PVN neurons and regulate not only feeding, but also peripheral tissue metabolism. This ARC–PVN signal controlling the liver metabolism and BAT thermogenesis activation has been previously reported in response to other stimuli.[45–47]

In contrast, the free (±)-C75-CoA did not induce neuronal activation in the PVN but reduced c-FOS in the ARC (Fig. 6E), the latter being related to a reduction of NPY-expressing neurons, contributing to the satiating effect of the free drug. The lack of neuronal activation in the PVN could explain the fact that the free drug did not reduce body weight nor alter the expression of genes related to liver metabolism and BAT thermogenesis. The differences observed between the nanomedicine and the free drug in the expression of hypothalamic neuropeptides, neuronal activation and in turn peripheral metabolism could also be related to the higher degree of uptake shown by the nanomedicine in the neurons compared to the free cargo in the cell cultures and the capacity of the nanomedicine to reach hypothalamic areas regulating energy balance (Fig. S6, ESI†).

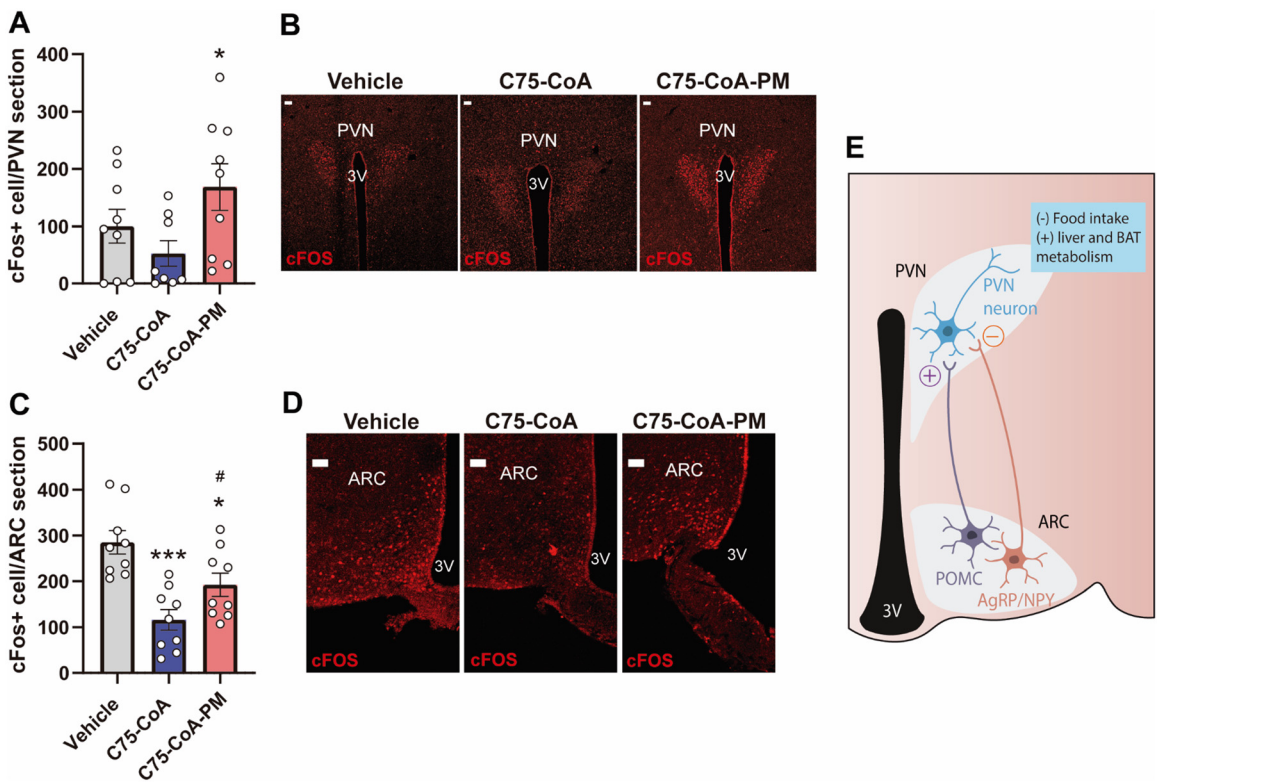

Fig. 6 Neuronal activation in the arcuate (ARC) and paraventricular (PVN) hypothalamic nuclei by ICV administration of (±)-C75-CoA polymeric micelles (PM). (A) Quantification and (B) representative confocal images showing c-FOS positive cells in the PVN section. (C) Quantification and (D) representative confocal images showing cFOS positive cells in the ARC section. (E) Schematic representation of ARC and PVN nuclei and the main types of neurons regulating energy balance. POMC activates PVN neurons leading to anti-obesity actions, whereas NPY neurons lead to a PVN inhibitory signal to promote feeding and body weight gain. Animals were perfused and the brains were collected 2 h post-injection of vehicle, free (±)-C75-CoA or (±)-C75-CoA-PM. Scale bars, 50 μm. Data are expressed as mean ± SD (3 animals, 3 slices per animal). Means were compared using one-way ANOVA along with Tukey's *post hoc* test. $*p < 0.05$ and $***p < 0.001$ *vs.* vehicle. $^{\#}p < 0.05$ *vs.* free (±)-C75-CoA.

3. Conclusion

In this study, we have developed an inventive core crosslinked micelle-based approach to successfully encapsulate and centrally deliver a CPT1A inhibitor, to acutely regulate energy balance in mice. The effective delivery and higher neuronal uptake of the drug was evidenced by the potent and rapid satiating effect and significant body weight loss induced by the central administration of (±)-C75-CoA-PM in mice, as well as by the substantial regulation of appetite-related hypothalamic neuropeptides and neuronal activation of the PVN, which were not observed in response to the free (±)-C75-CoA treatment. Altogether, the present study showcases the first nanomedicine targeting brain lipid metabolism, offering an innovative and selective therapeutic approach for treating diseases related to dysregulation of energy balance such as obesity and diabetes. The findings of this study are expected to contribute to the corroboration and advancement of the novel prospects of nanomedicine-based approaches to modulate body weight and feeding by targeting brain lipid metabolism. Most significantly, the current study highlights the enormous potential of nanotechnology in healthcare, leading the way for a better understanding of energy balance in the early stages of obesity and diabetes that are crucial for understanding the developmental stages of these pathological conditions and thus finding an effective cure.

4. Experimental section

4.1 Preparation of the polymers and crosslinked micelles

4.1.1 Synthesis of the triblock copolymer, PEG-PBLA-PLys (TFA). The synthesis of the triblock co-polymer, PEG-PBLA-PLys(TFA), was carried out by *N*-carboxyanhydride (NCA) ring-opening polymerization (ROP), as previously reported[51,52] but with modifications (Fig. 2). The initiator used in the first ROP step was α-methoxy-ω-amino-poly(ethylene glycol) (M_w: 12 kDa; PEG-NH_2, NOF, Japan), to produce the PEG-poly(β-benzyl-L-aspartate) diblock copolymer (PEG-PBLA). PEG-NH_2 was dried overnight *in vacuo* and dissolved in distilled and dehydrated DMF (Wako Pure Chemical Industries, Japan). BLA-NCA (24 molar equivalence to PEG-NH_2) and thiourea (equivalent to 1 M solution in DMF) were added to the PEG-NH_2 solution as a dry powder under an inert atmosphere. The mixture was left to stir at 25 °C for 24 h. The resulting reaction mixture was dialyzed against water and the PEG-PBLA-NH_2 di-block polymer was recovered by freeze-drying. The freeze-dried di-block polymer was dissolved in dichloromethane and dropped in a mixture of *n*-hexane and ethyl acetate (6 : 4), followed by filtration of the precipitated polymer, and drying under vacuum. The degree of polymerization was found to be 22 BLA units by ^{1}H NMR.

The obtained PEG-PBLA-NH_2 was subsequently used as an initiator for the second ROP of Lys(TFA)-NCA to obtain PEG-PBLA-PLys(TFA). PEG-PBLA-NH_2 was dried overnight *in vacuo* and subsequently dissolved in distilled and dehydrated DMSO. Lys(TFA)-NCA (44 molar equivalence to PEG-PBLA-NH_2) along with thiourea (equivalent to 1 M solution in DMF) was introduced to the PEG-PBLA-NH_2 solution as a dry powder under an Ar atmosphere, where the mixture was left to react at 25 °C for 48 h. The resulting reaction mixture was dialyzed against water and the PEG-PBLA-PLys(TFA) triblock polymer was recovered by freeze-drying. The freeze-dried triblock polymer was dissolved in methanol and subjected to diethyl ether precipitation and was finally dried *in vacuo*. For characterization purposes, an aliquot of the polymer was subjected to alkali hydrolysis to remove the benzyl esters and TFA groups, furnishing a water-soluble form of the triblock (PEG-PAsp-PLys) polymer. Upon ^{1}H NMR analysis of this PEG-PAsp-PLys polymer, it was revealed that 40 units of lysine residues were added with 22 units of aspartate (Fig. S8A, ESI†). Gel Permeation Chromatography (GPC) analysis (Jasco HPLC system equipped with an RI detector) confirmed (Fig. S8A, ESI†) that the polymer, PEG-PAsp-Plys, has a narrow and unimodal distribution of molecular weight (molecular weight distribution, M_w/M_n: 1.02).

4.1.2 Middle-block modification of PEG-PBLA-PLys(TFA) and the subsequent sequential deprotection. PEG-PBLA-PLys (TFA) was dissolved in anhydrous DMF (Sigma-Aldrich, cat. # 227056-100ML), to which an aromatic aminoacetal linker, 1-[4-(dimethoxymethyl)phenyl]methanamine (Enamine Ltd (Kyiv, Ukraine) (30 eq.)) was added. The reaction mixture was stirred at 40 °C for 72 h. Then, deprotection of the PLys(TFA) chain was carried out by adding 3 mL of methanol and 100 μL of 5 N NaOH. The reaction was allowed to proceed overnight. The mixture was then dialyzed against 0.02 N HCl (3×) and water (2×) for 48 h using a 8 kDa molecular weight cutoff (MWCO) dialysis bag (Spectra/Por, Spectrum Laboratories, cat. # 25223-650). The solution was freeze-dried under vacuum to obtain the modified triblock co-polymer (PEG-PAsp(Aldehyde)-PLys). ^{1}H NMR analysis confirmed the introduction of benzaldehyde groups onto the triblock polymer (Fig. S8B, ESI†).

4.1.3 Preparation of PEG-PAsp(hydrazide) and PEG-PLys. The synthesis of PEG-PBLA and its hydrazinolysis were carried out as previously reported,[53] while PEG-PLys was prepared similar to a previous study.[54] The preparation of labelled polymers and FRET micelles is detailed in the ESI.†

4.1.4 Micelle preparation. The crosslinked PM was formed by automatic self-assembly of polymers with the anionic drug cargo plus the hydrazone bond formation between the polymers. Polymer solutions were each dispersed in 10 mM phosphate buffer (PB) (pH 5.0) at 10 mg mL^{-1} concentration. The solutions were simply mixed with 36.87 mM (±)-C75-CoA or 7.88 mM Fluor-CoA (preparations of which are fully described in our previous work[28]) to attain a 1 : 1 anion/cation ratio, diluted with 10 mM PB (pH 7.4) to the desired concentration, and then vortexed. The micelle was allowed to cross-link at 4 °C for 24 h before passing through a 0.22 μM syringe filter (Millex 13 mm Durapore, Merck, cat. # SLGVJ13SL). The characterization of micelles is indicated in the ESI.†

4.2 Mouse cannulation and administration of drugs and polymeric micelles

The protocols for animal care and use were approved by the Ethics and Research Committee at the University of Barcelona (procedure ref. 10906 from the Generalitat de Catalunya). All experimental animal procedures were carried out in strict accordance with the European Communities directive 2010/63/EU legislation regulating animal research. All efforts were devoted to minimize animal suffering and to reduce the number of animals used.

Male (8–10 weeks old) C57BL/6J mice were used for the experiments. All animals were housed under conditions of a 12 h/12 h light/dark cycle (from 8 am to 8 pm) in a temperature- and humidity-controlled room, and allowed free access to water and standard laboratory chow. For fasting experiments, animals were randomly assigned to food-deprived (fasted group) or fed *ad libitum* groups (fed group). For tissue collection, animals were sacrificed by cervical dislocation under isoflurane anaesthesia during the light phase and the hypothalamus, liver and adipose tissue were quickly removed and stored at −80 °C.

For cannulation, cannulae were stereotaxically implanted into the lateral cerebral ventricle under anaesthesia, as previously described.[55,56] Cannulated mice were subjected to 16 h fasting before the beginning of the dark cycle. After that, mice were exposed to food and randomly assigned to the following treatments: 3 μl of vehicle (PBS), (±)-C75, (±)-C75-CoA, (±)-C75-CoA-PM (at 4.2 mM cargo concentration; injection dosage: 126.5 μg per mouse), Fluor-CoA or Fluor-CoA-PM (at 2.95 mM cargo concentration; injection dosage: 104 μg per mouse) by ICV injection 30 min before the beginning of the dark cycle. The schedule of this protocol was based on previous publications analysing feeding pattern after ICV administration of drugs.[13,14] The dosage of (±)-C75 in the free form or PM form was also based on previous studies.[13,22,24]

For feeding experiments, food intake was monitored at 1, 2, 4, 8, 12 and 24 hours after ICV administration, whereas body weight was measured before and 24 hours after the treatment. For tissue collection and gene expression analysis, food intake and body weight were monitored 2 h after drug administration and the mice were subsequently euthanized. Fresh tissues were then harvested and stored at −80 °C.

For brain immunofluorescence, mice were anesthetized using ketamine/xylazine and intracardially perfused with PBS and then with 10% NBF at 2 hours after (±)-C75-CoA, (±)-C75-CoA-PM, Fluor-CoA or Fluor-CoA-PM treatment. Brains were collected and post-fixated 24 h in 10% NBF at 4 °C, transferred to 30% sucrose at 4 °C for 2–3 days, frozen in isopentane, and sliced into 30 μm thick slices in the coronal plane throughout the entire rostral–caudal extent of the brain using a cryostat. The subsequent analysis for brain immunofluorescence or RT-PCR in the tissues is detailed in the ESI.†

4.3 Statistical analysis

All results are expressed as mean ± SD. Statistical analysis was conducted using GraphPad Prism 9 Software (GraphPad Software, La Jolla, CA, USA). Statistical analysis was performed by ANOVA (more than 2 groups were compared) followed by Tukey's *post-hoc* test. $p < 0.05$ was considered statistically significant. The number of animals used in each experiment is specified in each figure legend.

Author contributions

Conceptualization: S. Q. and R. R.-R.; methodology: J. G.-C., W. K. D. P., S. Z., A. F., A. C. R., S. A., L. S.-G., S. F. and K. T.; investigation: J. G.-C., W. K. D. P., X. A., S. Q. and R. R.-R.; visualization: J. G.-C., W. K. D. P., S. Q. and R. R.-R; supervision: S. Q., R. R.-R., X. A. and K. K.; writing – original draft: J. G.-C., W. K. D. P., S. Q. and R. R.-R.; writing – review and editing: W. K. D. P., S. Q., R. R.-R., X. A., N. C., D. S., L. H., J. G., K. K.

Conflicts of interest

There are no conflicts to declare.

Acknowledgements

This project was financially supported by the Joint Bilateral Project Japan-Spain (PCI2018-092997 to R. R.-R.)/Agencia Estatal de Investigación (AEI) and (20jm0210059h0003 to S. Q.)/Agency for Medical Research and Development (AMED), the Japan Society for Promotion of Science (JSPS) Bilateral Joint Research Projects (JPJSBP120209938 to S. Q.), and the Center of Innovation (COI) Program (JPMJCE1305) from Japan Science and Technology Agency (JST). This study was also supported by the Ministerio de Ciencia e Innovación (MCIN/AEI/10.13039/501100011033) (PID2020-114953RB-C22 to N. C. and R. R.-R.; PID2020-114953RB-C21 to L. H. and D. S.) co-funded by the European Regional Development Fund [ERDF], the Biomedical Research Centre in Pathophysiology of Obesity and Nutrition (CIBEROBN) (grant CB06/03/0001 to L. H.), and the Merck Health Foundation (to L. H.).

The authors would like to thank Dr Yuki Mochida (Innovation Center of Nanomedicine) for his help in obtaining the TEM images.

References

1 I. González-García, J. Fernø, C. Diéguez, R. Nogueiras and M. López, *Neuroendocrinology*, 2017, **104**, 398–411.
2 World Health Organization, Obesity and overweight, **https://www.who.int/news-room/fact-sheets/detail/obesity-and-overweight**, (accessed 19 November 2019).
3 V. S. Malik, W. C. Willet and F. B. Hu, *Nat. Rev. Endocrinol.*, 2020, **16**, 615–616.
4 K. Timper and J. C. Brüning, *Dis. Models Mech.*, 2017, **10**, 679–689.

5 T. Scherer, K. Sakamoto and C. Buettner, *Nat. Rev. Endocrinol.*, 2021, **17**, 468–483.
6 P. Dimitri, *Front. Endocrinol.*, 2022, **13**, e846880.
7 A. Fosch, S. Zagmutt, N. Casals and R. Rodríguez-Rodríguez, *Int. J. Mol. Sci.*, 2021, **22**, 6186.
8 M. López, C. J. Lelliott and A. Vidal-Puig, *BioEssays*, 2007, **29**, 248–261.
9 S. Obici, Z. Feng, K. Morgan, D. Stein, G. Karkanias and L. Rossetti, *Diabetes*, 2002, **51**, 271–275.
10 M. López, R. Nogueiras, M. Tena-Sempere and C. Diéguez, *Nat. Rev. Endocrinol.*, 2016, **12**, 421–432.
11 K. D. Bruce, A. Zsombok and R. H. Eckel, *Front. Endocrinol.*, 2017, **8**, 60.
12 I. R. Schlaepfer and M. Joshi, *Endocrinology*, 2020, **161**, 1–14.
13 Z. Hu, S. H. Cha, S. Chohnan and M. D. Lane, *Proc. Natl. Acad. Sci. U. S. A.*, 2003, **100**, 12624–12629.
14 Z. Hu, Y. Dai, M. Prentki, S. Chohnan and M. D. Lane, *J. Biol. Chem.*, 2005, **280**, 39681–39683.
15 T. K. T. Lam, A. Pocai, R. Gutierrez-Juarez, S. Obici, J. Bryan, L. Aguilar-Bryan, G. J. Schwartz and L. Rossetti, *Nat. Med.*, 2005, **11**, 320–327.
16 R. Fadó, R. Rodríguez-Rodríguez and N. Casals, *Prog. Lipid Res.*, 2021, **81**, 101071.
17 J. M. Orellana-Gavaldà, L. Herrero, M. I. Malandrino, A. Pañeda, M. Sol Rodríguez-Peña, H. Petry, G. Asins, S. Van Deventer, F. G. Hegardt and D. Serra, *Hepatology*, 2011, **53**, 821–832.
18 M. Weber, P. Mera, J. Casas, J. Salvador, A. Rodríguez, S. Alonso, D. Sebastián, M. C. Soler-Vázquez, C. Montironi, S. Recalde, R. Fucho, M. Calderón-Domínguez, J. F. Mir, R. Bartrons, J. C. Escola-Gil, D. Sánchez-Infantes, A. Zorzano, V. Llorente-Cortes, N. Casals, V. Valentí, G. Frühbeck, L. Herrero and D. Serra, *FASEB J.*, 2020, **34**, 11816–11837.
19 R. Rodríguez-Rodríguez, A. Fosch, J. Garcia-Chica, S. Zagmutt and N. Casals, *J. Neuroendocrinol.*, 2023, DOI: **https://doi.org/10.1111/jne.13234**.
20 J. Dai, K. Liang, S. Zhao, W. Jia, Y. Liu, H. Wu, J. Lv, C. Cao, T. Chen, S. Zhuang, X. Hou, S. Zhou, X. Zhang, X. W. Chen, Y. Huang, R. P. Xiao, Y. L. Wang, T. Luo, J. Xiao and C. Wang, *Proc. Natl. Acad. Sci. U. S. A.*, 2018, **115**, E5896–E5905.
21 S. Obici, Z. Feng, A. Arduini, R. Conti and L. Rossetti, *Nat. Med.*, 2003, **9**, 756–761.
22 P. Mera, A. Bentebibel, E. López-Viñas, A. G. Cordente, C. Gurunathan, D. Sebastián, I. Vázquez, L. Herrero, X. Ariza, P. Gómez-Puertas, G. Asins, D. Serra, J. García and F. G. Hegardt, *Biochem. Pharmacol.*, 2009, **77**, 1084–1095.
23 S. Gao and M. D. Lane, *Proc. Natl. Acad. Sci. U. S. A.*, 2003, **100**, 5628–5633.
24 T. M. Loftus, D. E. Jaworsky, G. L. Frehywot, C. A. Townsend, G. V. Ronnett, M. D. Lane and F. P. Kuhajda, *Science*, 2000, **288**, 2379–2381.
25 S. H. Cha, Z. Hu and M. D. Lane, *Biochem. Biophys. Res. Commun.*, 2004, **317**, 301–308.
26 K. Makowski, P. Mera, D. Paredes, L. Herrero, X. Ariza, G. Asins, F. G. Hegardt, J. García and D. Serra, *Chirality*, 2013, **25**, 281–287.
27 M. C. Cheng, X. H. Qiang and C. M. Du, *Chin. Sci. Bull.*, 2013, **58**, 1256–1261.
28 W. K. D. Paraiso, J. Garcia-Chica, X. Ariza, S. Zagmutt, S. Fukushima, J. Garcia, Y. Mochida, D. Serra, L. Herrero, H. Kinoh, N. Casals, K. Kataoka, R. Rodríguez-Rodríguez and S. Quader, *Biomater. Sci.*, 2021, **9**, 7076–7091.
29 S. Quader, X. Liu, K. Toh, Y. L. Su, A. R. Maity, A. Tao, W. K. D. Paraiso, Y. Mochida, H. Kinoh, H. Cabral and K. Kataoka, *Biomaterials*, 2021, **267**, e120463.
30 H. Shibasaki, H. Kinoh, H. Cabral, S. Quader, Y. Mochida, X. Liu, K. Toh, K. Miyano, Y. Matsumoto, T. Yamasoba and K. Kataoka, *ACS Nano*, 2021, **15**, 5545–5559.
31 H. J. Kim, K. Miyata, T. Nomoto, M. Zheng, A. Kim, X. Liu, H. Cabral, R. J. Christie, N. Nishiyama and K. Kataoka, *Biomaterials*, 2014, **35**, 4548–4556.
32 H. Cabral, K. Miyata, K. Osada and K. Kataoka, *Chem. Rev.*, 2018, **118**, 6844–6892.
33 J. W. McFadden, S. Aja, Q. Li, V. V. R. Bandaru, E. K. Kim, N. J. Haughey, F. P. Kuhajda and G. V. Ronnett, *PLoS One*, 2014, **9**, e115642.
34 S. H. Cha, Z. Hu, S. Chohnan and M. D. Lane, *Proc. Natl. Acad. Sci. U. S. A.*, 2005, **102**, 14557–14562.
35 S. H. Cha, J. T. Rodgers, P. Puigserver, S. Chohnan and M. D. Lane, *Proc. Natl. Acad. Sci. U. S. A.*, 2006, **103**, 15410–15415.
36 Z. Hu, H. C. Seung, G. Van Haasteren, J. Wang and M. D. Lane, *Proc. Natl. Acad. Sci. U. S. A.*, 2005, **102**, 3972–3977.
37 H. C. Seung, M. Wolfgang, Y. Tokutake, S. Chohnan and M. D. Lane, *Proc. Natl. Acad. Sci. U. S. A.*, 2008, **105**, 16871–16875.
38 M. S. Vohra, K. Benchoula, C. J. Serpell and W. E. Hwa, *Eur. J. Pharmacol.*, 2022, **915**, 174611.
39 C. Quarta, M. Claret, L. M. Zeltser, K. W. Williams, G. S. H. Yeo, M. H. Tschöp, S. Diano, J. C. Brüning and D. Cota, *Nat. Metab.*, 2021, **3**, 299–308.
40 M. V. Kumar, T. Shimokawa, T. R. Nagy and M. D. Lane, *Proc. Natl. Acad. Sci. U. S. A.*, 2002, **99**, 1921–1925.
41 M. Schneeberger, R. Gomis and M. Claret, *J. Endocrinol.*, 2014, **220**, T25–T46.
42 E. Roh, D. K. Song and M. S. Kim, *Exp. Mol. Med.*, 2016, **48**, e216–e216.
43 C. Contreras, R. Nogueiras, C. Diéguez, K. Rahmouni and M. López, *Redox Biol.*, 2017, **12**, 854–863.
44 T. Yoneshiro, R. Rodríguez-Rodríguez, M. J. Betz and P. C. N. Rensen, *Front. Endocrinol.*, 2020, **11**, 845.
45 C. Contreras, I. González-García, P. Seoane-Collazo, N. Martínez-Sánchez, L. Liñares-Pose, E. Rial-Pensado, J. Fernø, M. Tena-Sempere, N. Casals, C. Diéguez, R. Nogueiras and M. López, *Diabetes*, 2017, **66**, 87–99.
46 L. P. Klieverik, S. F. Janssen, A. Van Riel, E. Foppen, P. H. Bisschop, M. J. Serlie, A. Boelen, T. Ackermans, H. P. Sauerwein, E. Fliers and A. Kalsbeek, *Proc. Natl. Acad. Sci. U. S. A.*, 2009, **106**, 5966–5971.

47 M. T. Hackl, C. Fürnsinn, C. M. Schuh, M. Krssak, F. Carli, S. Guerra, A. Freudenthaler, S. Baumgartner-Parzer, T. H. Helbich, A. Luger, M. Zeyda, A. Gastaldelli, C. Buettner and T. Scherer, *Nat. Commun.*, 2019, **10**, 2717.
48 A. Bonaccorso, T. Musumeci, M. F. Serapide, R. Pellitteri, I. F. Uchegbu and G. Puglisi, *Colloids Surf., B*, 2017, **154**, 297–306.
49 S. Dante, A. Petrelli, E. M. Petrini, R. Marotta, A. Maccione, A. Alabastri, A. Quarta, F. De Donato, T. Ravasenga, A. Sathya, R. Cingolani, R. Proietti Zaccaria, L. Berdondini, A. Barberis and T. Pellegrino, *ACS Nano*, 2017, **11**, 6630–6640.
50 R. Rodriguez-Rodriguez and S. Quader, *Nanomedicine*, 2022, **17**, 495–498.
51 S. Fukushima, K. Miyata, N. Nishiyama, N. Kanayama, Y. Yamasaki and K. Kataoka, *J. Am. Chem. Soc.*, 2005, **127**, 2810–2811.
52 K. Miyata, M. Oba, M. Nakanishi, S. Fukushima, Y. Yamasaki, H. Koyama, N. Nishiyama and K. Kataoka, *J. Am. Chem. Soc.*, 2008, **130**, 16287–16294.
53 S. Quader, H. Cabral, Y. Mochida, T. Ishii, X. Liu, K. Toh, H. Kinoh, Y. Miura, N. Nishiyama and K. Kataoka, *J. Controlled Release*, 2014, **188**, 67–77.
54 K. Osada, T. Shiotani, T. A. Tockary, D. Kobayashi, H. Oshima, S. Ikeda, R. J. Christie, K. Itaka and K. Kataoka, *Biomaterials*, 2012, **33**, 325–332.
55 R. Rodríguez-Rodríguez, C. Miralpeix, A. Fosch, M. Pozo, M. Calderón-Domínguez, X. Perpinyà, M. Vellvehí, M. López, L. Herrero, D. Serra and N. Casals, *Mol. Metab.*, 2019, **19**, 75–85.
56 M. Pozo, R. Rodrguez-Rodrguez, S. Raḿrez, P. Seoane-Collazo, M. López, D. Serra, L. Herrero and N. Casals, *Endocrinology*, 2017, **158**, 2226–2238.